



# Metal–organic framework derived Pd/ZrO<sub>2</sub>@CN as a stable catalyst for the catalytic hydrogenation of 2,3,5-trimethylbenzoquinone

Shasha Li | Jianping Pan | Xiaoxue Wu | Yanghe Fu | Qiang Xiao | Fumin Zhang | Weidong Zhu

Key Laboratory of the Ministry of Education for Advanced Catalysis Materials, Institute of Physical Chemistry, Zhejiang Normal University, 321004 Jinhua, People's Republic of China

## Correspondence

Fumin Zhang and Weidong Zhu, Key Laboratory of the Ministry of Education for Advanced Catalysis Materials, Institute of Physical Chemistry, Zhejiang Normal University, 321004 Jinhua, People's Republic of China.

Email: zhangfumin@zjnu.edu.cn; weidongzhu@zjnu.cn

## Funding information

National Natural Science Foundation of China, Grant/Award Numbers: 21576243, No. 21576243; Zhejiang Provincial Natural Science Foundation of China, Grant/Award Number: LY18B060006, LY18B030006 LY18B030006, Nos. LY18B060006

Metal–organic frameworks (MOFs) have recently been identified as versatile sacrificing templates to construct functional nanomaterials for heterogeneous catalysis. Herein, we report a thermal transformation strategy to directly fabricate metal Pd nanoclusters inlaid within a ZrO<sub>2</sub>@nitrogen-doped porous carbon (Pd/ZrO<sub>2</sub>@CN) composite using Pd@NH<sub>2</sub>-UiO-66(Zr) as a precursor that was pre-synthesized by a one-pot hydrothermal method. The developed Pd/ZrO<sub>2</sub>@CN as a robust catalyst delivered remarkable stability and activity to the catalytic hydrogenation of 2,3,5-trimethylbenzoquinone (TMBQ) to 2,3,5-trimethylhydroquinone (TMHQ), a key reaction involved in vitamin E production. The hydrogenation was carried out at 110 °C with 1.0 MPa H<sub>2</sub>, and it resulted in 98% TMHQ yield as the sole product over five consecutive cycles, outperforming the analogue Pd/ZrO<sub>2</sub>@C without nitrogen doping templated from Pd@UiO-66(Zr). The excellent catalytic properties of Pd/ZrO<sub>2</sub>@CN likely originated from the highly stable ultrafine Pd nanoclusters inlaid within ZrO<sub>2</sub>@CN matrix on account of the strong interaction between N and Pd, as well as on the Lewis acidity of ZrO<sub>2</sub>, which was beneficial to the hydrogenation.

## KEYWORDS

2,3,5-trimethylbenzoquinone, catalytic hydrogenation, MOF-derived catalyst, NH<sub>2</sub>-UiO-66(Zr), Pd nanoclusters

## 1 | INTRODUCTION

Catalytic hydrogenation is an important type of reaction in modern chemical industrial and petroleum refining, in which catalysts play a central role.<sup>[1–4]</sup> Compared to homogeneous catalysts, heterogeneous catalysts are frequently used in large-scale production processes by virtue of their convenient recycling and repeated usability.<sup>[1–4]</sup> So far, noble metal heterogeneous catalysts, despite their high cost and scarcity, are still regarded as the most efficient hydrogenation catalysts because of their high

catalytic activity.<sup>[5–8]</sup> However, aggregation or leaching of those noble metal species inevitably occurs during the practical application of conventional supported catalysts,<sup>[9]</sup> especially in liquid-phase reactions. Therefore, the development of highly stable and active noble metal-based heterogeneous catalysts for the hydrogenation reaction is still highly desired, but it is a huge challenge.

Metal–organic frameworks (MOFs), a relatively new class of ordered porous materials built by assembling metal ions/clusters and rigid organic linkers, have proven

to be advanced functional materials for a wide variety of applications.<sup>[10–12]</sup> MOFs have also attracted remarkable attention as promising sacrificial precursors for the preparation of porous carbon and/or metal oxide nanocomposite materials via high-temperature thermal transformation.<sup>[13–16]</sup> The various atoms that periodical alternation in MOFs renders congenial conditions for evenly atomic arrangements.<sup>[10,17]</sup> Therefore, nitrogen-functionalized organic linkers in well-defined MOFs would guarantee uniform distribution of the resulting nitrogen atoms within the network of a porous carbon matrix upon high-temperature treatment under an inert atmosphere.<sup>[18]</sup> In addition, the coexisting metal oxide in the derived functional nanomaterials can tune the surface electronic structures of noble metal nanoclusters and thus modify the catalytic properties of the derived composite catalysts.<sup>[19]</sup> Nevertheless, development of a feasible and facile methodology to directly establish noble metal nanoclusters inlaid within a metal oxide/nitrogen-doped porous carbon composite as a highly stable catalyst is seldom reported.

In a previous work, we reported a strategy for the construction of a composite made of Pd nanoclusters in a NH<sub>2</sub>-functionalized MOF [Pd@NH<sub>2</sub>-UiO-66(Zr)] using an optimized temperature control program. In this process, chelation of Pd ions with the amine groups, in situ assembly of ZrCl<sub>4</sub> and 2-aminoterephthalic acid (NH<sub>2</sub>-BDC) containing Pd ions, and an on-site reduction process were integrated into one step.<sup>[20]</sup> By virtue of the abundant cavities in the MOF and the coordination capability of the amine groups, the Pd nanoclusters were well distributed within the NH<sub>2</sub>-UiO-66 cavities over the obtained Pd@NH<sub>2</sub>-UiO-66(Zr). Thus, Pd@NH<sub>2</sub>-UiO-66(Zr) showed a high catalytic activity in the hydrogenation of 2,3,5-trimethylbenzoquinone (TMBQ) to 2,3,5-trimethylhydroquinone (TMHQ),<sup>[20]</sup> a key reaction for the production of vitamin E.<sup>[21–23]</sup> However, compared to conventional supports, such as metal oxides and porous carbon, the thermal and/or chemical stabilities of the MOF-based catalysts are still relatively low,<sup>[10–12]</sup> thus impeding their practical usage, particularly for catalytic reactions carried out under relatively harsh conditions.

Bearing the above discussion in mind, herein, we report a thermal transformation strategy to directly fabricate metal Pd nanoclusters inlaid within a ZrO<sub>2</sub>@nitrogen-doped porous carbon (Pd/ZrO<sub>2</sub>@CN) composite using Pd@NH<sub>2</sub>-UiO-66(Zr) as the sacrificial precursor. After systematic characterizations, the prepared Pd/ZrO<sub>2</sub>@CN was applied to the hydrogenation of TMBQ to TMHQ under elevated temperature and pressure conditions (110 °C, 1.0 MPa H<sub>2</sub>). By virtue of the strong interaction between the lone-pair electrons of the

N species and the 5d empty orbitals of the Pd ions, as well as to the Lewis acidity of ZrO<sub>2</sub>, which promotes hydrogenation, the resulting Pd/ZrO<sub>2</sub>@CN exhibited good recyclability and reactivity.

## 2 | EXPERIMENTAL

### 2.1 | Catalyst preparation

#### 2.1.1 | Synthesis of Pd@NH<sub>2</sub>-UiO-66(Zr)<sup>[20]</sup>

The precursor Pd@NH<sub>2</sub>-UiO-66(Zr) was synthesized by a facile one-pot strategy without adding any external reducing agent. Typically, ZrCl<sub>4</sub> (1.0 g, 4.3 mmol), NH<sub>2</sub>-BDC (0.78 g, 4.3 mmol), acetic acid (30 ml), and deionized water (3.0 ml) were dissolved in dimethylformamide (DMF) (160 ml) in a glass flask (250 ml capacity). To accelerate the dissolution of the reactants, the slurry was first subjected to ultrasonication treatment for 10 min. Then, the Pd precursor (0.03 mol/l, 2.0 ml) was added dropwise into the solution. The mixture was stirred at 35 °C for 7 hr. Subsequently, the temperature was increased to 75 °C and stirred for an additional 20 hr. Afterwards, the temperature was elevated to 130 °C and stirring continued for another 4 hr. The obtained solid was then washed with DMF and methanol three times and then dried at 150 °C for 12 hr. NH<sub>2</sub>-UiO-66(Zr), UiO-66(Zr), and Pd@UiO-66(Zr) were also synthesized by following the same procedure described above using the appropriate precursors.

#### Preparation of Pd/ZrO<sub>2</sub>@CN

The Pd/ZrO<sub>2</sub>@CN powders were fabricated directly via a high-temperature thermal transformation treatment. Typically, the Pd@NH<sub>2</sub>-UiO-66(Zr) crystals (2.0 g) were transferred into a tube furnace. The furnace was heated at 700 °C at a rate of 1 °C/min with nitrogen gas flow (flow rate: 80 ml/min). The furnace was held at this temperature for 2 hr and then allowed to cool to room temperature. With the heating treatment under N<sub>2</sub> flow, the Pd@NH<sub>2</sub>-UiO-66(Zr) was converted into a Pd/ZrO<sub>2</sub>@CN nanocomposite, which was then used as the hydrogenation catalyst. ZrO<sub>2</sub>@CN, ZrO<sub>2</sub>@C, and Pd/ZrO<sub>2</sub>@C were prepared following the same procedure.

The methods for the catalyst characterizations are provided in the Supporting Information.

### 2.2 | Hydrogenation of TMBQ

The catalytic hydrogenation reaction was carried out in a high-pressure Teflon-lined autoclave (50 ml, NS50-MP-LT-SS1-SV-BS, Anhui Kemi Machinery Technology Co.

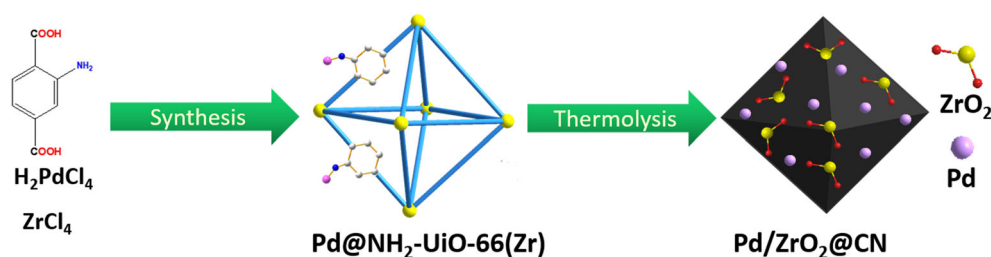
Ltd., Anhui, China). Typically, TMBQ (0.54 g), catalyst (0.05 g), and *i*-propanol (15 ml) as the solvent were placed in the autoclave and repeatedly purged with H<sub>2</sub> (10 times) at 25 °C. The autoclave was then heated quickly to the given reaction temperature (110 °C), after which hydrogen was introduced and a constant pressure (1.0 MPa) was maintained in the reactor. Finally, agitation was initiated with a stirring speed of 1000 rpm. The reaction mixtures were analyzed regularly by using a gas chromatography (Shimadzu 2014) equipped with a flame ionization detector and an InertCap 5 capillary column. The recyclability of the Pd/ZrO<sub>2</sub>@CN catalyst was tested after its separation from the reaction system by centrifugation, rinsing with a large quantity of ethanol, and drying in a vacuum desiccator at 150 °C for 8 hr.

### 3 | RESULTS AND DISCUSSION

Scheme 1 shows a schematic illustration of the preparation of Pd/ZrO<sub>2</sub>@CN. The MOF chosen for accommodating the Pd nanoclusters was NH<sub>2</sub>-UiO-66(Zr) [Zr<sub>6</sub>O<sub>4</sub>(OH)<sub>4</sub>(NH<sub>2</sub>-BDC)<sub>6</sub>], which features substantial coordination sites (amine groups), abundant cavities, and a large specific surface area.<sup>[24,25]</sup> Pd@NH<sub>2</sub>-UiO-66(Zr) can be conveniently synthesized by a one-pot strategy. By further pyrolysis at high temperature under an

inert atmosphere, the organic linkers and inorganic Zr-based anodes of NH<sub>2</sub>-UiO-66(Zr) were converted into nitrogen-doped porous carbon and ZrO<sub>2</sub> nanoparticles, respectively. The -NH<sub>2</sub> groups in the formed MOFs are vital for the fabrication of ultra-small Pd nanoclusters as these groups can largely impede the migration of Pd nanoclusters at high temperatures owing to the strong interaction between the lone-pair electrons of the N species and the 5d empty orbitals of the Pd ions.<sup>[26–29]</sup> In contrast, without the assistance of the -NH<sub>2</sub> groups, the Pd species were inclined to aggregate into relatively large nanoparticles upon pyrolysis of the counterpart Pd@UiO-66(Zr).

The powder XRD patterns of Pd@NH<sub>2</sub>-UiO-66(Zr) were almost identical to those of the calculated UiO-66(Zr) (Figure 1a),<sup>[23–25]</sup> demonstrating that Pd@NH<sub>2</sub>-UiO-66(Zr) was successfully synthesized via the temperature control program described above. Upon carbonizing treatment at 700 °C under N<sub>2</sub> flow, the peaks of NH<sub>2</sub>-UiO-66(Zr) completely vanished and new peaks ascribed to tetragonal ZrO<sub>2</sub> appeared (Figure 1a). No characteristic peaks of Pd nanoclusters were observed, implying that the Pd nanoclusters were likely highly dispersed in the derived ZrO<sub>2</sub>@CN. In addition, the absence of XRD peaks associated with crystallized carbon demonstrated that the generated carbon species were amorphous. In contrast, for the corresponding Pd/ZrO<sub>2</sub>@C derived from



**SCHEME 1** Schematic illustration for preparation of the Pd/ZrO<sub>2</sub>@CN catalyst.

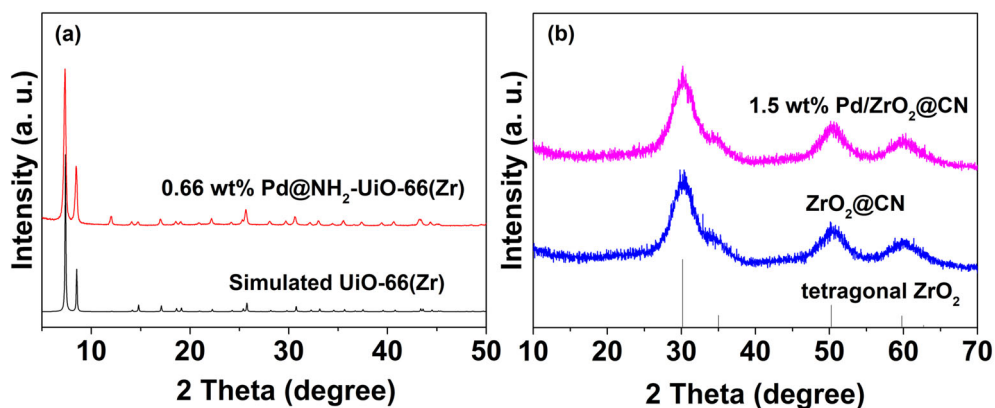


**FIGURE 1** Powder XRD patterns of various samples

Pd@UiO-66(Zr) under the same conditions, a sharp diffraction peak at around 40 °C ascribed to the Pd species was clearly observed (Figures S1 and S2 in the Supporting Information), suggesting that the Pd species significantly aggregated during the thermal transformation procedure. This comparison demonstrates that amine groups are indispensable for the dispersion of ultra-small Pd nanoclusters.<sup>[26–29]</sup> Further calculations using the Scherrer equation revealed that the size of the Pd nanoparticles in Pd/ZrO<sub>2</sub>@C was about 13 nm. ICP-AES analysis showed that the actual Pd loadings in Pd/ZrO<sub>2</sub>@CN and Pd/ZrO<sub>2</sub>@C were 1.5 wt% and 1.1 wt%, respectively (Table S1 in the Supporting Information).

The specific surface areas of various samples were measured via the N<sub>2</sub> adsorption experiment at –196 °C (Figure 2 and Table S1).<sup>[24,25]</sup> Upon high-temperature pyrolysis, the precursor Pd@NH<sub>2</sub>-UiO-66(Zr) was converted into Pd/ZrO<sub>2</sub>@CN, mainly induced by the thermal transformation of the organic linkers into nitrogen-doped porous carbon and the Zr-based nodes into ZrO<sub>2</sub>. The derived Pd/ZrO<sub>2</sub>@CN lost most its porosity, resulting in a relatively low specific surface area of 290.5 m<sup>2</sup>/g as compared to 906 m<sup>2</sup>/g of Pd@NH<sub>2</sub>-UiO-66(Zr). Scanning

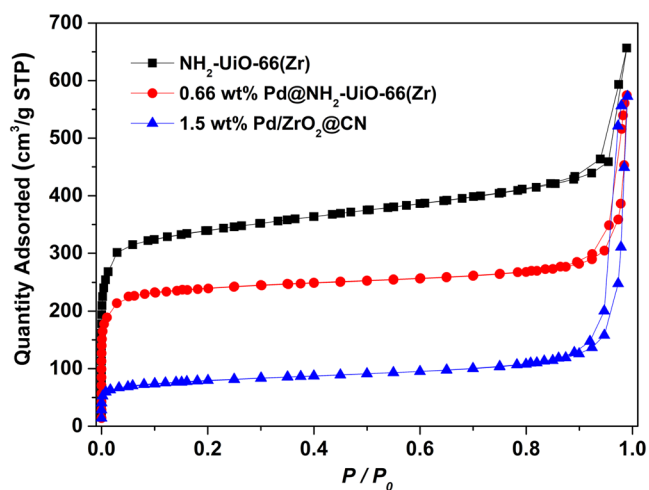


FIGURE 2 N<sub>2</sub> isotherms of various samples

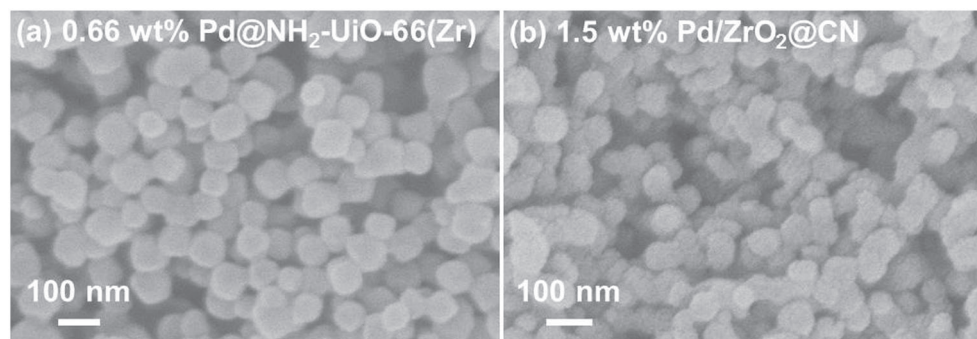
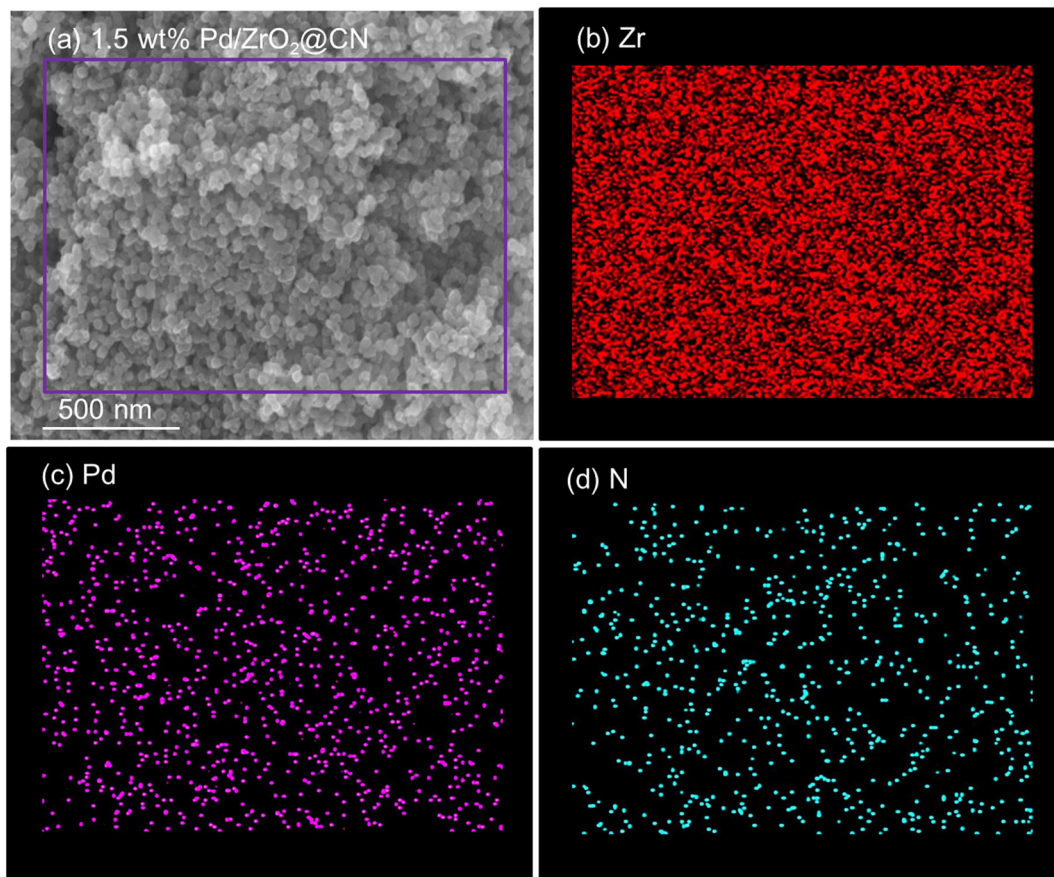


FIGURE 3 SEM photos of (a) Pd@NH<sub>2</sub>-UiO-66(Zr) and (b) Pd/ZrO<sub>2</sub>@CN

electron microscopy (SEM) photos revealed a relatively uniform octahedral morphology with a diameter of approximately 70–80 nm for the precursor Pd@NH<sub>2</sub>-UiO-66(Zr) (Figure 3).<sup>[23]</sup> As expected, the average crystal size of the Pd/ZrO<sub>2</sub>@CN slightly decreased as compared to the precursor due to the shrinkage during thermolysis treatment. EDS analysis suggested Pd, N, and Zr were well distributed throughout the Pd/ZrO<sub>2</sub>@CN (Figure 4). The embedded ZrO<sub>2</sub> nanoparticles, with an average size of 4–6 nm, were uniformly embedded within the ZrO<sub>2</sub>@CN (Figure 5), which corresponds well with the XRD results. The high-resolution transmission electron (HRTEM) microscopy image manifested some regular fringes, corresponding to the (111) planes of the tetragonal ZrO<sub>2</sub> phase (Figure 5).<sup>[30]</sup> Notably, no Pd nanoclusters were detected, revealing the high distribution of ultra-small Pd nanoclusters within ZrO<sub>2</sub>@CN. The slightly higher dispersion of Pd in Pd/ZrO<sub>2</sub>@CN than that in Pd/ZrO<sub>2</sub>@C was confirmed by the CO chemisorption experiments (Table S1).

XPS analyses of Pd/ZrO<sub>2</sub>@CN and Pd/ZrO<sub>2</sub>@C further indicated the existence of ZrO<sub>2</sub>, where the Zr 3p<sub>3/2</sub> and Zr 3p<sub>1/2</sub> peaks at 333.1 eV and 346.7 eV, respectively, are assigned Zr<sup>4+</sup> (Figure 6a and Figure 6b).<sup>[30]</sup> Moreover, the signals at 335.3 eV and 340.9 eV are attributed to the Pd 3d<sub>5/2</sub> and Pd 3d<sub>3/2</sub> levels, respectively, of Pd<sup>0</sup> in Pd/ZrO<sub>2</sub>@C (Figure 6a).<sup>[23]</sup> However, these peaks slightly negative shifted in the Pd 3d spectra of Pd/ZrO<sub>2</sub>@CN (Figure 6b),<sup>[23–25]</sup> mostly due to the strong interaction between the Pd species and N during the high-temperature pyrolysis. To further verify this interaction, the N species in Pd/ZrO<sub>2</sub>@C and Pd/ZrO<sub>2</sub>@CN were also characterized by XPS (Figure 6c and Figure 6d). The peak at 401.1 eV was assigned to graphitic N. The pyridinic N (400.1 eV) and pyrrolic N (398.5 eV) peaks were dominant in the Pd/ZrO<sub>2</sub>@CN (Figure 6d). These two types of N atoms were coexisted in a  $\pi$ -conjugated system, which as anchor centers could stabilize the Pd nanoclusters.<sup>[28]</sup> Previous studies implied that N doping in porous carbon could effectively generate a large



**FIGURE 4** EDS mapping for Pd/ZrO<sub>2</sub>@CN

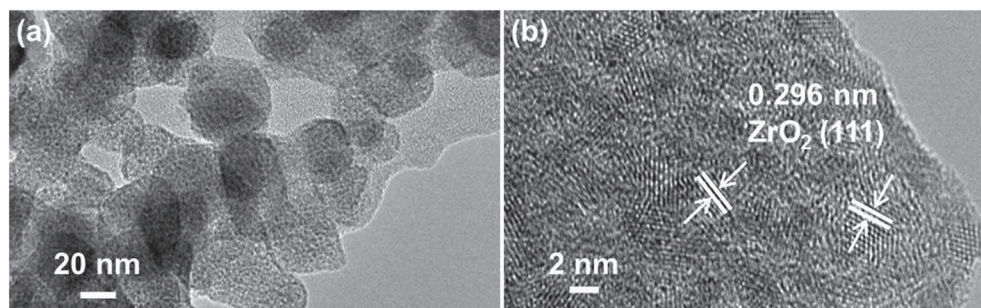


**FIGURE 5** TEM images of Pd/ZrO<sub>2</sub>@CN

number of topological defects, and the corresponding density is associated with the intensity ratio of the D and G bands ( $I_D/I_G$ ) in the Raman spectra.<sup>[28,31]</sup> The  $I_D/I_G$  values for Pd/ZrO<sub>2</sub>@CN and Pd/ZrO<sub>2</sub>@C were calculated to be 1.3 and 0.9, respectively (Figure 7). This supports the hypothesis that there would be more dispersive defects in Pd/ZrO<sub>2</sub>@CN, which might help stabilize the Pd nanoclusters. Based on the above analysis, it can be concluded that the Pd/ZrO<sub>2</sub>@CN catalyst with a uniform dispersion of ultra-small Pd nanoclusters was successfully prepared by the thermal transformation method. As a comparison, Pd/ZrO<sub>2</sub>@C with a similar morphology, Pd loading, and specific surface area but with a severe aggregation of Pd nanoparticles was also

obtained by the same method (Table S1 and Figures S1–S6).

With the Pd/ZrO<sub>2</sub>@CN catalyst in hand, we then evaluated its catalytic performance in the catalytic hydrogenation of TMBQ to TMHQ, an important transformation for vitamin E production, as a model reaction. When the initial concentration of TMBQ increased from 0.23 mol/l to 2.33 mol/l (i.e., the molar ratio of TMBQ to metal Pd was set to be 500, 2,000, and 5,000, respectively), the conversion rate of TMBQ decreased gradually (Figure 8). This may have been due to the fact that the total number of hydrogenation active sites in the fixed catalyst dosage (0.05 g) remained constant; that is, the conversion rate of the reactant per unit time did not

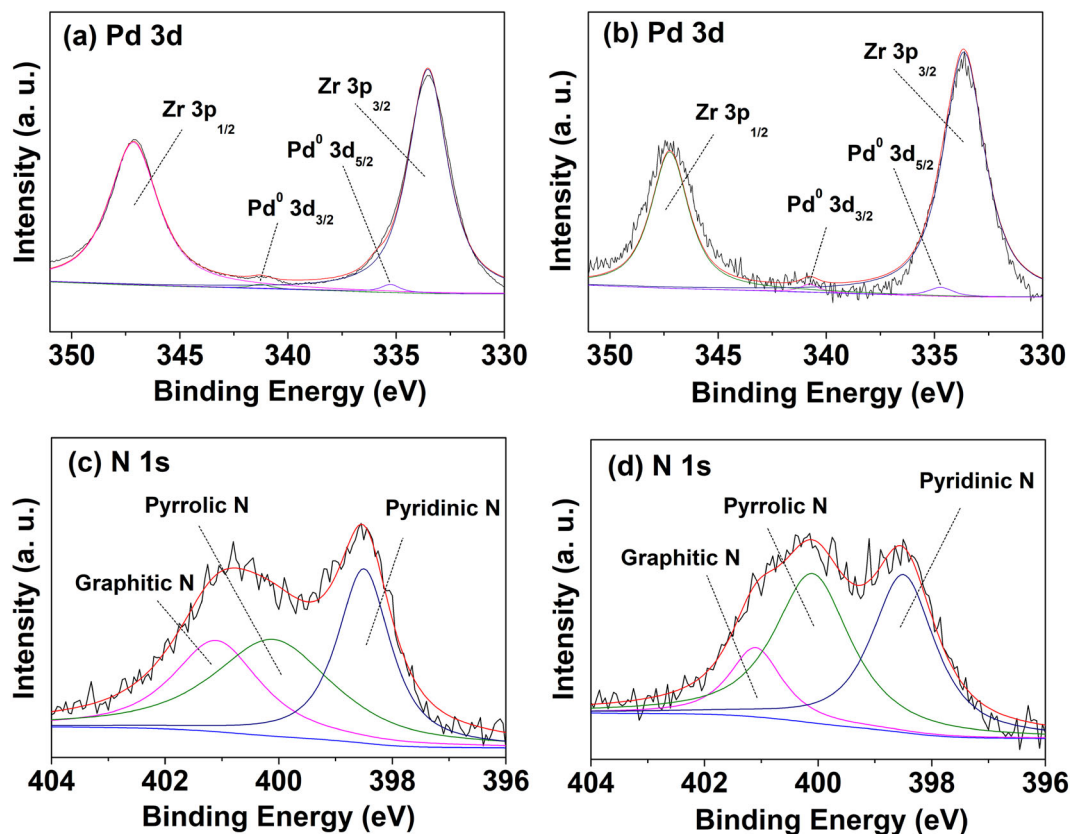


**FIGURE 6** High-resolution XPS spectra: Zr and Pd spectra of (a) Pd/ZrO<sub>2</sub>, (b) Pd/ZrO<sub>2</sub>@CN; N spectrum of (c) ZrO<sub>2</sub>@C and (d) Pd/ZrO<sub>2</sub>@CN

improve upon reaching the maximum. Further increases in the initial concentration of TMBQ caused the relative consumption of the reactants per unit time to decrease, and thus the overall conversion rate dropped with the increase of the initial TMBQ concentration.

As can be seen from Figure 9a, the conversion rate of TMBQ increased significantly with increasing reaction temperature, mainly owing to the fact that the high

temperature helped accelerate the activation of the reactants. Because the reaction time needed for complete conversion at the lower temperature was relatively longer, 110 °C is selected as the optimum temperature in further studies. As shown in Figure 9b, when the hydrogen pressure was increased from 0.5 to 1.0 MPa, the conversion

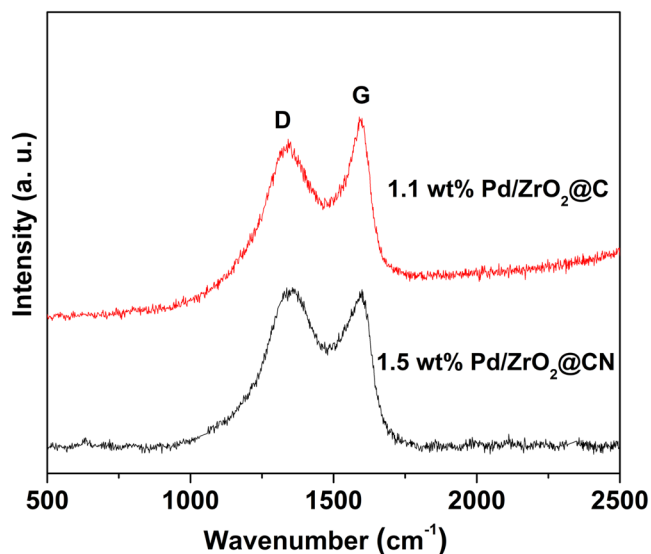


**FIGURE 7** Raman spectra of Pd/ZrO<sub>2</sub>@CN and Pd/ZrO<sub>2</sub>@C

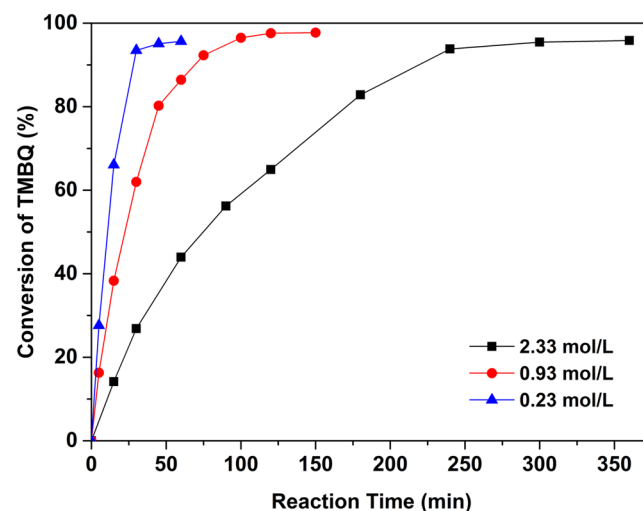


**FIGURE 8** Influence of TMBQ initial concentrations on the conversion of TMBQ as a function of reaction time. Reaction conditions: TMBQ (0.54 g), 1.5 wt% Pd/ZrO<sub>2</sub>@CN (0.05 g), *i*-propanol (15 ml), 1.0 MPa H<sub>2</sub>, 110 °C

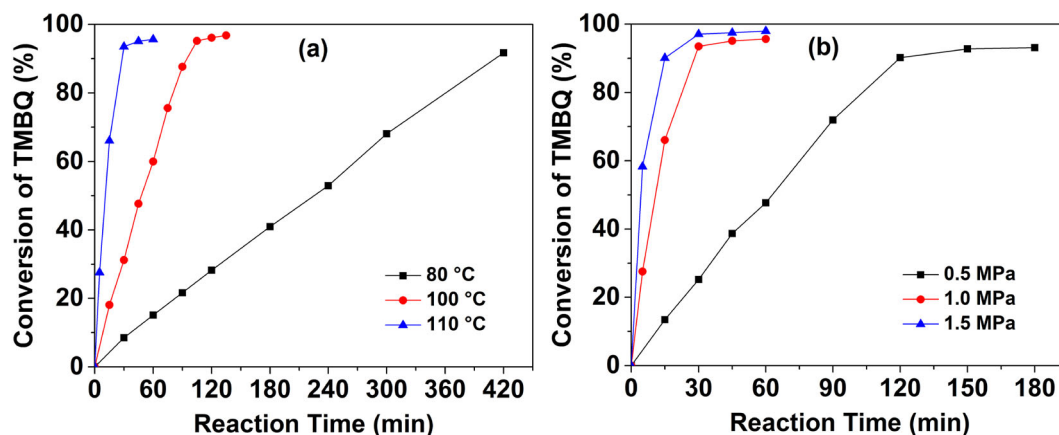


**FIGURE 9** Conversion of TMBQ as a function of reaction time under different (a) reaction temperatures and (b) hydrogen pressures. Reaction conditions: (a) TMBQ (0.54 g), 1.5 wt% Pd/ZrO<sub>2</sub>@CN (0.05 g), *i*-propanol (15 ml), 1.0 MPa H<sub>2</sub>; (b) TMBQ (0.54 g), 1.5 wt% Pd/ZrO<sub>2</sub>@CN (0.05 g), *i*-propanol (15 ml), 110 °C

rate of TMBQ increased significantly. With a further increase of the hydrogen pressure up to 1.5 MPa, although the initial conversion rate of TMBQ increased to some extent, this trend became less pronounced after reaction of 30 min. Therefore, in the further investigations, the reactions were performed at a hydrogen pressure of 1.0 MPa. In addition, the catalytic activity of Pd/ZrO<sub>2</sub>@CN was also compared with the analogue Pd/ZrO<sub>2</sub>@C without nitrogen atom doping (Figure 10). Only a trace amount of TMBQ was converted when the reaction was conducted in the absence of a catalyst (blank experiment) or over the bare ZrO<sub>2</sub>@CN support (not shown). Pd/ZrO<sub>2</sub>@CN showed a TMBQ conversion of 66%, with TMHQ as the sole product at 110 °C and 1.0 MPa of hydrogen pressure for 15 min. Furthermore, 95% TMBQ conversion was achieved when the reaction time was increased to 45 min (Figure 10). In contrast,

Pd/ZrO<sub>2</sub>@C exhibited a much lower catalytic activity of TMBQ under a same reaction condition. In addition to the appropriate acidity of ZrO<sub>2</sub> that promote the hydrogenation,<sup>[22,23]</sup> the superior catalytic activity of Pd/ZrO<sub>2</sub>@CN could be mainly ascribed to the highly dispersed Pd nanoclusters within the ZrO<sub>2</sub>@CN support compared to that of Pd/ZrO<sub>2</sub>@C,<sup>[21]</sup> as confirmed by the XRD and TEM analyses.

The recyclability of the heterogeneous catalysts is crucial for their practical application. We further tested the stability of 1.5 wt% Pd/ZrO<sub>2</sub>@CN. There was no obvious decrease in catalytic activity over five cycles, regardless whether the reaction was performed for 15 or 45 min, demonstrating the excellent stability of the prepared 1.5 wt% Pd/ZrO<sub>2</sub>@CN catalyst for the hydrogenation of TMBQ (Figure 11). The recovered catalysts were further analyzed by N<sub>2</sub> adsorption (Table S1), Pd dispersion (Table S1), TEM (Figure 12), EDS mapping (Figure 13),

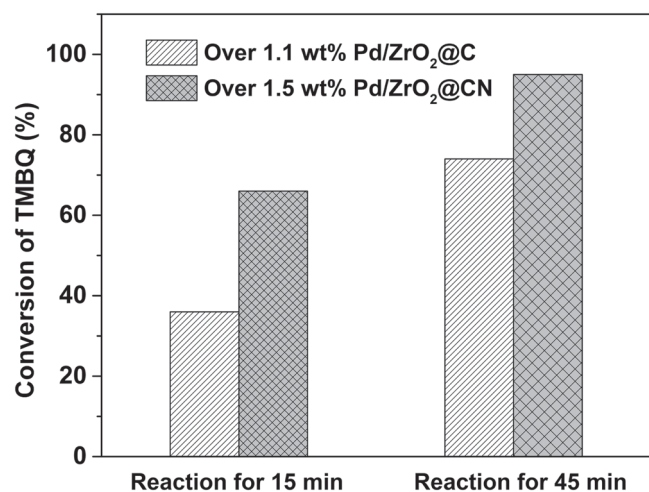


**FIGURE 10** Activity comparison between 1.5 wt% Pd/ZrO<sub>2</sub>@CN and 1.1 wt% Pd/ZrO<sub>2</sub>@C. Reaction conditions: TMBQ (0.54 g), molar ratio of TMBQ to Pd in the catalyst is 500, *i*-propanol (15 ml), 1.0 MPa H<sub>2</sub>, 110 °C

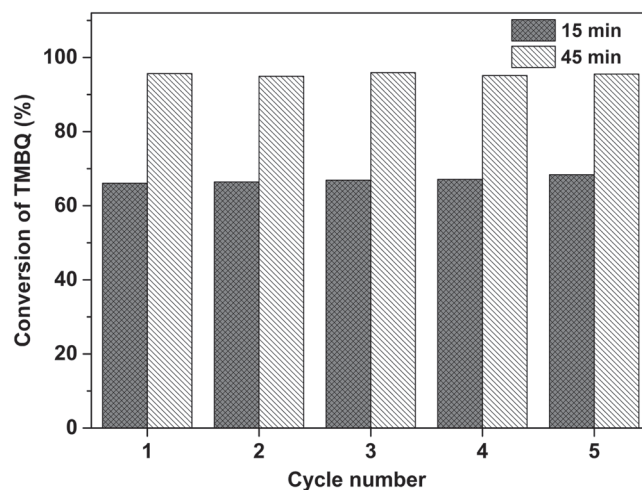


**FIGURE 11** Recyclability of 1.5 wt% Pd/ZrO<sub>2</sub>@CN. Reaction conditions: TMBQ (0.54 g), catalyst (50 mg), 110 °C, 1.0 MPa H<sub>2</sub>

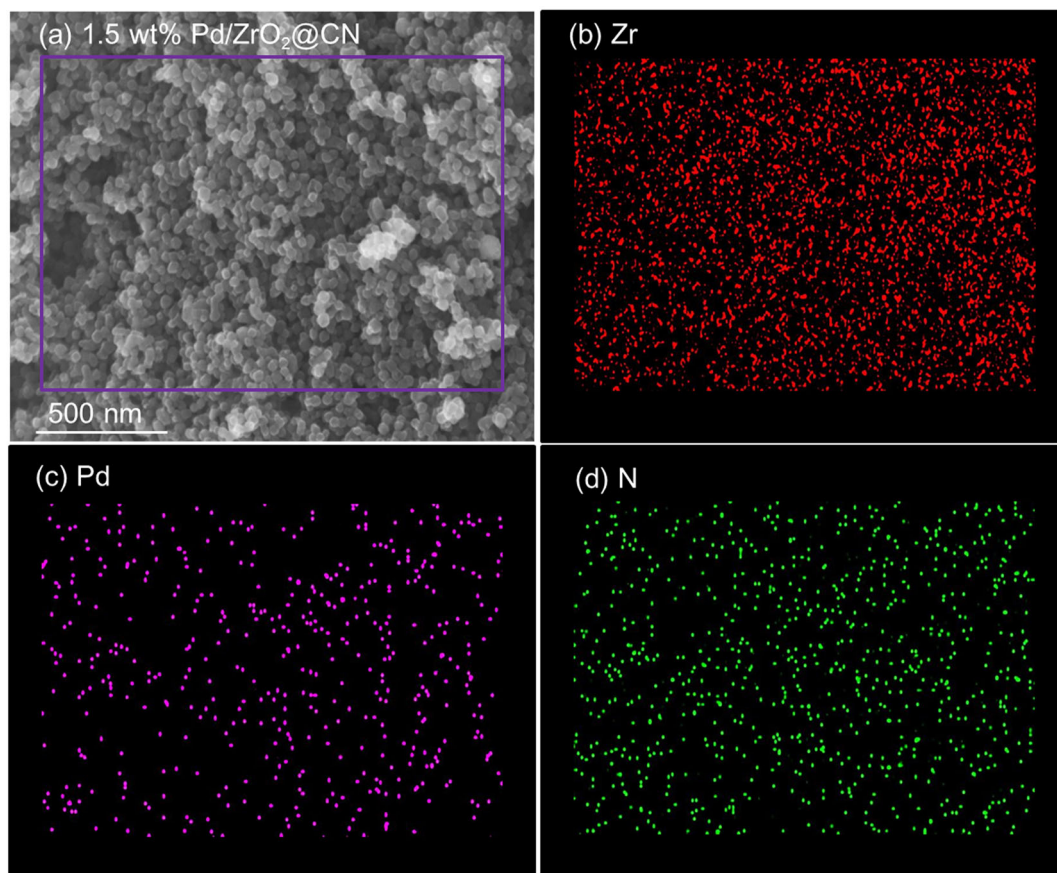


FIGURE 12 SEM and EDS mapping of the used 1.5 wt% Pd@ZrO<sub>2</sub>@CN

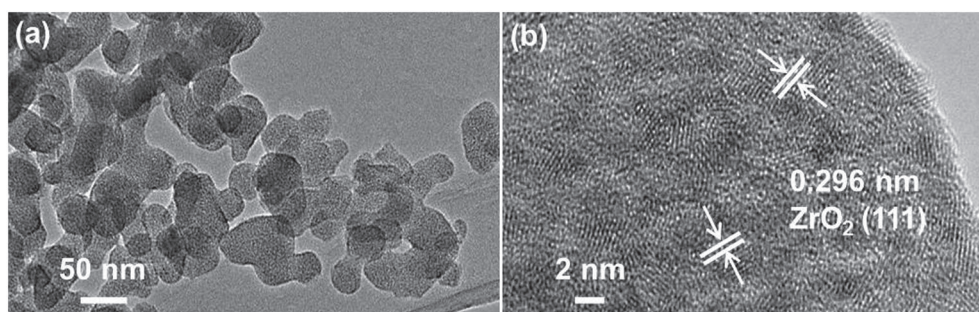


FIGURE 13 TEM and HRTEM images of the used 1.5 wt% Pd@ZrO<sub>2</sub>@CN

and Raman spectroscopy (Figure S7). The results revealed that there was no obvious difference in morphology, particle size, or distribution of Pd nanoclusters as compared to the fresh one, consistently confirming that Pd/ZrO<sub>2</sub>@CN was stable under the current reaction conditions.

#### 4 | CONCLUSIONS

In summary, highly dispersed Pd nanoclusters embedded within a matrix of ZrO<sub>2</sub>@CN were successfully prepared via direct pyrolysis of the precursor Pd@NH<sub>2</sub>-UiO-

66(Zr). The derived Pd/ZrO<sub>2</sub>@CN catalyst exhibited good reusability and activity in the catalytic hydrogenation of TMBQ to TMHQ under the investigated reaction conditions (110 °C, 1.0 MPa H<sub>2</sub>), attributable to the strong interaction between N and Pd, as well as to the Lewis acidity of ZrO<sub>2</sub>, which promotes hydrogenation. This work demonstrates the feasibility of using various inlaid metal nanoclusters within metal oxide@nitrogen-doped porous carbon composites as robust catalysts with excellent stability for the various catalytic applications. However, the catalytic activity of Pd/ZrO<sub>2</sub>@CN was lower than that of Pd@NH<sub>2</sub>-UiO-66(Zr),<sup>[23]</sup> probably owing to the fact that there were carbon coatings on the outer surfaces of

the Pd nanoclusters during the high-temperature hydrolysis,<sup>[32]</sup> which on one hand could stabilize Pd nanoclusters against sintering and leaching under harsh reaction conditions, but on the other could partial block the active sites. In further work, we will explore efficient strategies to remove the as-called carbon layer without affecting the size or morphology of the metal nanoclusters to boost the catalytic activity of the Pd nanoclusters while retaining their stability.

## ACKNOWLEDGEMENTS

Financial support from the National Natural Science Foundation of China (No. 21576243), and Zhejiang Provincial Natural Science Foundation of China (Nos. LY18B060006 and LY18B030006) are greatly appreciated.

## ORCID

Fumin Zhang  <https://orcid.org/0000-0003-1997-991X>

## REFERENCES

- [1] Y. Chen, Z. Wang, S. Mao, Y. Wang, *Chin. J. Catal.* **2019**, *40*, 971.
- [2] A. Wang, J. Li, T. Zhang, *Nat. Rev. Chem.* **2018**, *2*, 65.
- [3] N. Mizuno, M. Misono, *Chem. Rev.* **1998**, *98*, 199.
- [4] L. Liu, A. Corma, *Chem. Rev.* **2018**, *118*, 4981.
- [5] I. S. Kim, Z. Li, J. Zheng, A. E. Platero-Prats, A. Mavrandonakis, S. Pellizzeri, M. Ferrandon, A. Vjunov, L. C. Gallington, T. E. Webber, N. A. Vermeulen, R. L. Penn, R. B. Getman, C. J. Cramer, K. W. Chapman, D. M. Camaioni, J. L. Fulton, J. A. Lercher, O. K. Farha, J. T. Hupp, A. B. F. Martinson, *Angew. Chem. Int. Ed.* **2018**, *57*, 909.
- [6] Z. Zhang, Y. Zhu, H. Asakura, B. Zhang, J. Zhang, M. Zhou, Y. Han, T. Tanaka, A. Wang, T. Zhang, N. Yan, *Nat. Commun.* **2017**, *8*, 16100.
- [7] P. Liu, Y. Zhao, R. Qin, S. Mo, G. Chen, L. Gu, D. M. Chevrier, P. Zhang, Q. Guo, D. Zang, B. Wu, G. Fu, N. Zheng, *Science* **2016**, *352*, 797–801.
- [8] L. Yuwen, F. Xu, B. Xue, Z. Luo, Q. Zhang, B. Bao, S. Su, L. Weng, W. Huang, L. Wang, *Nanoscale* **2014**, *6*, 5762.
- [9] F. Su, F. Y. Lee, L. Lv, J. Liu, X. N. Tian, X. S. Zhao, *Adv. Funct. Mater.* **2007**, *17*, 1926.
- [10] L. Jiao, Y. Wang, H. L. Jiang, Q. Xu, *Adv. Mater.* **2018**, *30*, e1703663.
- [11] D. Yang, S. O. Odoh, T. C. Wang, O. K. Farha, J. T. Hupp, C. J. Cramer, L. Gagliardi, B. C. Gates, *J. Am. Chem. Soc.* **2015**, *137*, 7391.
- [12] N. Stock, S. Biswas, *Chem. Rev.* **2012**, *112*, 933.
- [13] Y. Z. Chen, R. Zhang, L. Jiao, H. L. Jiang, *Coordin. Chem. Rev.* **2018**, *362*, 1.
- [14] K. Chen, Z. Sun, R. Fang, Y. Shi, H. M. Cheng, F. Li, *Adv. Funct. Mater.* **2018**, *28*, 1707592.
- [15] H. R. Kim, T. U. Yoon, S. I. Kim, J. An, Y. S. Bae, C. Y. Lee, *RSC Adv.* **2017**, *7*, 1266.
- [16] K. Shen, X. Chen, J. Chen, Y. Li, *ACS Catal.* **2016**, *6*, 5887.
- [17] L. Jiao, G. Wan, R. Zhang, H. Zhou, S. H. Yu, H. L. Jiang, *Angew. Chem. Int. Ed.* **2018**, *57*, 8525.
- [18] G. Huang, L. Yang, X. Ma, J. Jiang, S. H. Yu, H. L. Jiang, *Chem. – Eur. J.* **2016**, *22*, 3470.
- [19] K. Shen, L. Chen, J. Long, W. Zhong, Y. Li, *ACS Catal.* **2015**, *5*, 5264.
- [20] S. Zheng, P. Yang, F. Zhang, D. L. Chen, W. Zhu, *Chem. Eng. J.* **2017**, *328*, 977.
- [21] D. Su, Z. Wei, S. Mao, J. Wang, Y. Li, H. Li, Z. Chen, Y. Wang, *Catal. Sci. Technol.* **2016**, *6*, 4503.
- [22] X. Cai, J. Pan, G. Tu, Y. Fu, F. Zhang, W. Zhu, *Catal. Commun.* **2018**, *113*, 23.
- [23] X. Zhao, Y. Jin, F. Zhang, Y. Zhong, W. Zhu, *Chem. Eng. J.* **2014**, *239*, 33.
- [24] J. H. Cavka, S. Jakobsen, U. Olsbye, N. Guillou, C. Lamberti, S. Bordiga, K. P. Lillerud, *J. Am. Chem. Soc.* **2008**, *130*, 13850.
- [25] M. Kandiah, M. H. Nilsen, S. Usseglio, S. Jakobsen, U. Olsbye, M. Tilset, C. Larabi, E. A. Quadrelli, F. Bonino, K. P. Lillerud, *Chem. Mater.* **2010**, *22*, 6632.
- [26] F. Zhang, S. Zheng, Q. Xiao, Y. Zhong, W. Zhu, A. Lin, M. Samy El-Shall, *Green Chem.* **2016**, *18*, 2900.
- [27] Y. K. Hwang, D. Y. Hong, J. S. Chang, S. H. Jhung, Y. K. Seo, J. Kim, A. Vimont, M. Daturi, C. Serre, G. Férey, *Angew. Chem. Int. Ed.* **2008**, *47*, 4144.
- [28] X. Wang, W. Chen, L. Zhang, T. Yao, W. Liu, Y. Lin, H. Ju, J. Dong, L. Zheng, W. Yan, X. Zheng, Z. Li, X. Wang, J. Yang, D. He, Y. Wang, Z. Deng, Y. Wu, Y. Li, *J. Am. Chem. Soc.* **2017**, *139*, 9419.
- [29] L. Chen, X. Chen, H. Liu, C. Bai, Y. Li, *J. Mater. Chem. A* **2015**, *3*, 15259.
- [30] W. Cao, W. Luo, H. Ge, Y. Su, A. Wang, T. Zhang, *Green Chem.* **2017**, *19*, 2201.
- [31] T. Zhang, D. Zhang, X. Han, T. Dong, X. Guo, C. Song, R. Si, W. Liu, Y. Liu, Z. Zhao, *J. Am. Chem. Soc.* **2018**, *140*, 16936.
- [32] Y. Cao, B. Zhao, X. Bao, Y. Wang, *ACS Catal.* **2018**, *8*, 7077.

## SUPPORTING INFORMATION

Additional supporting information may be found online in the Supporting Information section at the end of the article.

**How to cite this article:** Li S, Pan J, Wu X, et al. Metal–organic framework derived Pd/ZrO<sub>2</sub>@CN as a stable catalyst for the catalytic hydrogenation of 2,3,5-trimethylbenzoquinone. *Appl Organometal Chem.* 2019;e5233. <https://doi.org/10.1002/aoc.5233>